ELSEVIER

Journal of Nuclear Materials 258–263 (1998) 1694–1699

journal of nuclear materials

Microchemical and microstructural changes of austenitic steels caused by proton irradiation following helium implantation

T. Fukuda [a,*], T. Aoki [b], Y. Isobe [b], T. Furuya [a], A. Hasegawa [c], K. Abe [c]

[a] *Technical Development Department, Nuclear Fuel Industries, Ltd., Tokai-mura, Naka-gun, Ibaraki-ken 319-11, Japan*
[b] *Engineering Services Div., Nuclear Fuel Industries, Ltd., Kumatori-cho, Sennan-gun, Osaka 590-04, Japan*
[c] *Department of Quantum Science and Energy Engineering, Tohoku University, Aramaki-aza-Aoba, Aoba-ku 980-77, Japan*

Abstract

In austenitic steels used for light water reactors, neutron irradiation induces the microchemical and microstructural changes in matrices and around grain boundaries, which are related to various property changes, such as irradiation hardening and irradiation assisted stress corrosion cracking (IASCC). These phenomena may also be important in fusion reactors, if austenitic steels are used in core components. The grain boundary segregation and the microstructural development depend on irradiation conditions, such as dpa levels, helium contents and temperatures, etc. The effects of helium, however, have not yet been clarified. This paper presents microchemical and microstructural changes in 304SS and XM-19 steel implanted with helium and irradiated with proton. The TEM disks were implanted with helium of 15 appm and irradiated with 2 MeV H_2^+ ion to about 1 dpa at 300°C. Chemical analysis was performed using Field Emission Transmission Electron Microscope (FE-TEM) and showed that the depletion of chromium at a grain boundary. However, the amount of the depletion strongly depended on both chemical compositions of the steels and helium contents. Observation by TEM also indicated that small cavities generated in both of the irradiated steels. Nucleation of these cavities may be mainly due to the effects of implanted helium prior to H_2^+ ion irradiation.

1. Introduction

Austenitic alloys used under neutron irradiated environment are generally known to suffer many kinds of degradation. Although there are many studies on Radiation Induced Segregation (RIS) [1,2] and void swelling at high temperatures (>400°C) simulating fast and fusion reactor conditions up to now, irradiation studies at low temperatures are very scarce [3,4]. Thus it seems useful to obtain data base for low temperature irradiation in order to fully understand RIS in austenitic alloys. In addition, evaluating the degradation at low temperatures is extremely important to operate Light Water Reactors (LWRs), because IASCC in core components made of austenitic stainless steels has become one of the most pressing problems. Besides, other irradiation damages such as nucleation of void, irradiation hardening and creation of gaseous cavity from (n,α) and (n,p) reactions may occur in the LWR components under long time operations.

According to the literature regarding to irradiation damage for austenitic alloys under fast reactor condition, mobility of point defects such as interstitial and vacancy increases at higher temperatures, which results in suppressing recombination of the defects. Accordingly, irradiation damage basically increases with increasing irradiation temperature. On the other hand, since mobility of the defects decreases at low temperature, irradiation induced degradation seems to be not so active under 400°C. However, phenomena of the degradation under 400°C have not been clarified. The present study is therefore focused on microchemical and microstructural changes of commercial purity 304SS and improved XM-19 steels at 300°C using light ion accelerator in order to simulate neutron irradiation.

* Corresponding author. Tel.: +81 29 287 8213; fax: +81 29 287 8222; e-mail: fukuda@nfi.co.jp.

0022-3115/98/$19.00
PII: S0022-3115(98)00338-9

Table 1
Chemical composition of the sample alloy (wt%)

Alloy type	C	Si	Mn	P	S	Ni	Cr	Mo	N	Nb	V	Fe
304SS	0.06	0.57	1.12	0.032	0.007	8.66	18.20	–	–	–	–	Bal.
XM-19	0.03	0.45	4.85	0.016	0.001	11.90	21.90	2.16	0.31	0.20	0.19	Bal.

2. Experimental procedure

The test alloys consisted of commercial purity 304SS and XM-19 steel. Results of chemical analysis of the steels are shown in Table 1. Cold-worked alloy sheets of 0.25 mm thickness were solution annealed at 1000°C for recrystallization. The grain sizes of these steel sheets were controlled to be under 10 μm, so as to find a suitable grain boundary for TEM examination. The irradiation samples were punched out into 3 mm diameter disks and electropolished to thin down the disks to 0.15 mm.

Irradiation was carried out using 3 MeV He^+ ion at room temperature, which simulates the effect of He generation during Ni(n,α), and 2 MeV H_2^+ ion at 300°C to produce displacement damage of 1 dpa at a dose rate of approximately 4×10^{-5} dpa/s. The ion particle of H_2^+ irradiated in the sample produces two protons. Two different He injection schedules were utilized in this experiment, namely, 15 and 2000 appm He were injected prior to H_2^+ ion irradiation, corresponding to the amount of He generation from Ni(n,α) reaction of about 1 cycle and life terminal of some core internals in LWR [5]. The depth distributions of pre-injected He atom concentrations and displacement damage were estimated using TRIM-85 code (Fig. 1). During H_2^+ irradiation, target temperature was controlled to be 300°C through beam heating and a heat panel placed at backside of the disk monitoring by infrared pyrometer. Irradiation beam probe was controlled to be 3 mm in diameter using a collimator. The energy degrader was used to make the distribution of injected He atoms uniform at depth ranging from 1.5 to 3.5 μm. To clarify the effect of helium pre-injection, only proton-irradiated sample was prepared for XM-19 steel.

Irradiated samples were thinned by ion sputtering from irradiated side and electro-chemically polished from backside. Chemical compositions at grain boundary and microstructure were examined using Field-Emission TEM (HITACHI HF-2000) and EDX (Kevex

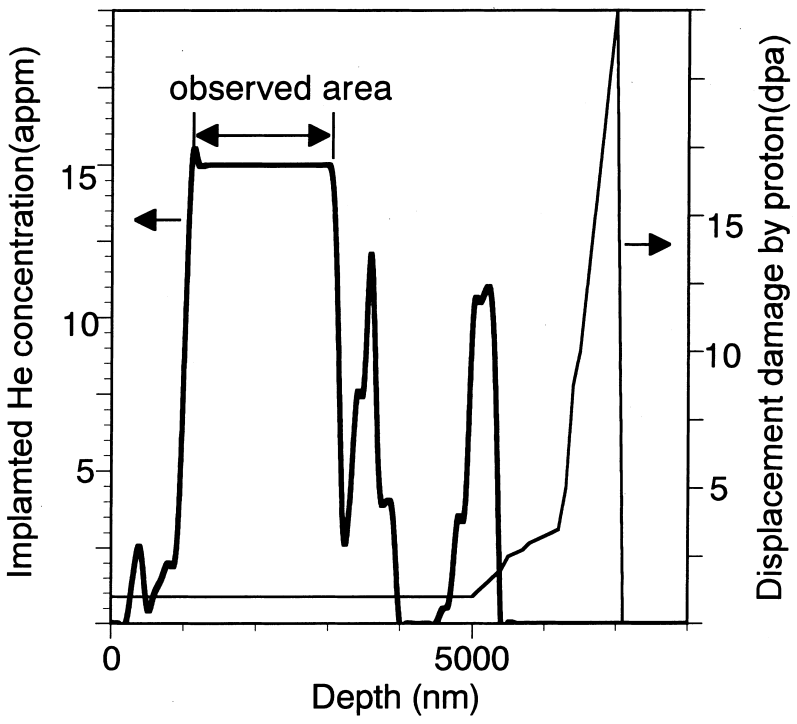

Fig. 1. Depth distribution of displacement damage and pre-injected He concentration calculated by the TRIM-85 code.

Delta-EDX). The thickness of TEM observed area was evaluated by Electron Energy Loss Spectroscopy (EELS). Quantitative analysis of the chemical composition was performed with the probe under 1 nm diameter.

3. Experimental results

3.1. Grain boundary segregation

Before chemical analysis at grain boundary, precipitation of chromium carbides at grain boundary was examined for unirradiated samples to distinguish segregation by irradiation from that by carbide formation, because the composition around the precipitate is generally different from that at no precipitate area. The result showed that no precipitation of chromium carbides occurred at grain boundary.

Drastic changes in alloy compositions were observed within 5 nm areas from irradiated grain boundary in each sample (Fig. 2). Analyzed elements were Fe, Ni, Cr, Si, P, S, Mn and Mo in the present study.

3.1.1. 304SS

Fig. 2(a) shows chemical analysis for 304SS pre-injected by He of 15 appm and irradiated by H_2^+ to 1 dpa, indicating that Cr was depleted from 18.2 wt% in the bulk to 10.7 wt% at grain boundary, and that Ni was enriched from 8.7 wt% in the bulk to 16.8 wt% at grain

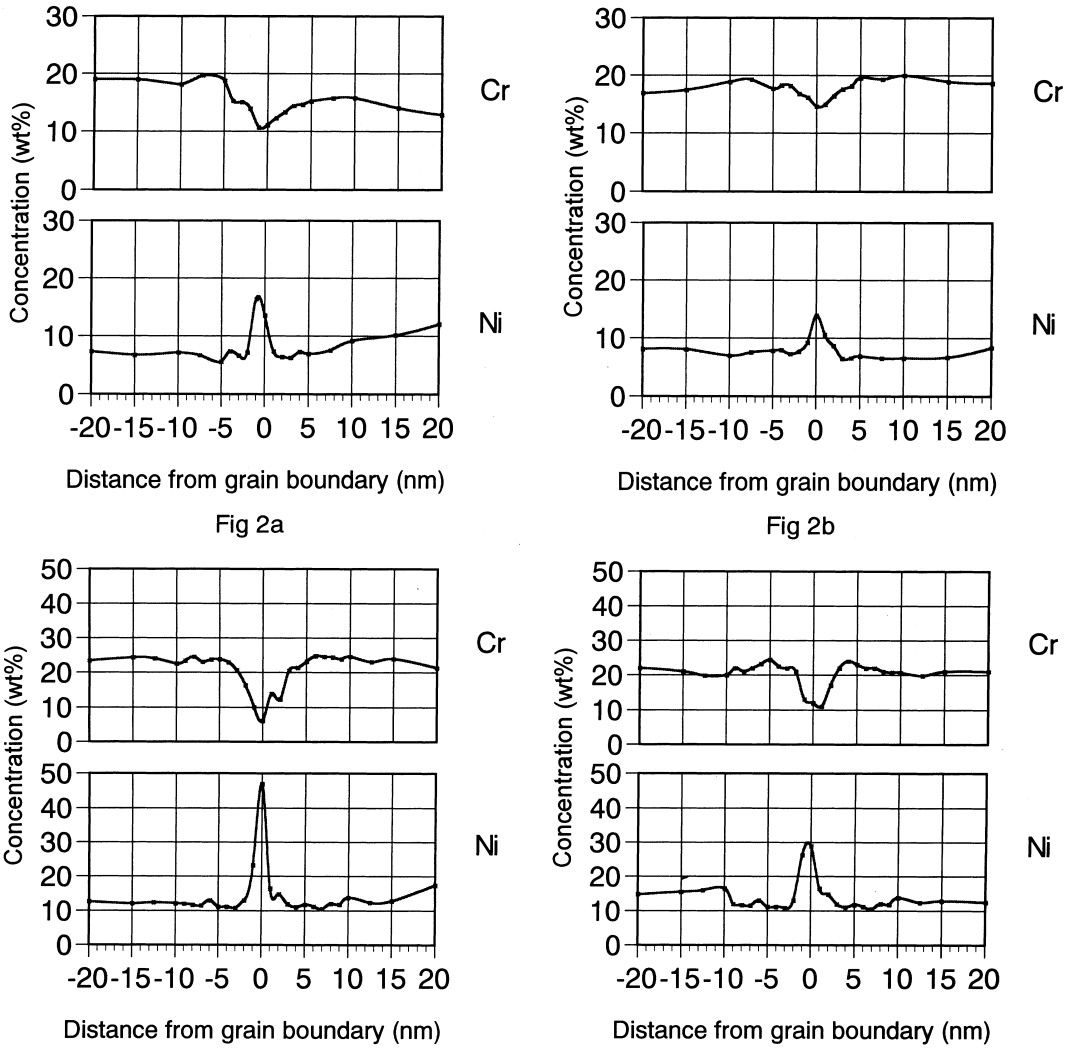

Fig. 2. Concentration of alloy composition near grainboundary (a) type 304SS He^+ pre-injected 15 appm and H_2^+ irradiated 1 dpa, (b) type 304SS He^+ pre-injected 2000 appm and H_2^+ irradiated 1 dpa, (c) type XM-19 He^+ pre-injected 15 appm and H_2^+ irradiated 1 dpa, (d) XM-19 He^+ pre-injected 2000 appm and H_2^+ irradiated 1 dpa.

Table 2
Summary of TEM measurements

Alloy type	Dose (dpa)	He concentration (appm)	Temperature (°C)	Cavity size (nm)	Swelling (%)	Cavity density (m^{-3})
304SS	1	15	300	4.9	0.03	5.21×10^{21}
	1	2000	300	4.7	0.07	1.37×10^{22}
XM-19	1	0	300	8.5	0.04	1.37×10^{21}
	1	15	300	10.3	0.72	1.42×10^{21}
	1	2000	300	3.5	0.06	3.5×10^{22}

boundary. Fig. 2(b) shows chemical analysis for 304SS pre-injected by He of 2000 appm and irradiated by H_2^+ to 1 dpa, indicating that Cr was depleted from 18.2 wt% in the bulk to 11.3 wt% at grain boundary, and that Ni was enriched from 8.7 wt% in the bulk to 16.5 wt% at grain boundary.

3.1.2. XM-19 steel

Fig. 2(c) shows chemical analysis for XM-19 steel pre-injected by He of 15 appm and irradiated by H_2^+ to 1 dpa, indicating that Cr was depleted from 21.9 wt% in the bulk to 6.7 wt% at grain boundary, and that Ni was enriched from 11.9 wt% in the bulk to 41.9 wt% at grain boundary. In addition depletion of Mn was observed at irradiated grain boundary. Fig. 2(d) shows chemical analysis for XM-19 steel pre-injected by He of 2000 appm and irradiated by H_2^+ to 1 dpa, indicating that Cr was depleted from 21.9 wt% in the bulk to 9.1 wt% at grain boundary, and that Ni was enriched from 11.9 wt% in the bulk to 33.8 wt% at grain boundary.

3.2. Microstructural observation

Results of TEM examination on microstructures and swelling were summarized in Table 2, where swelling was measured by TEM observations. Swelling is expressed by

$$\mathrm{Sw} = \frac{\Delta V}{V_{\mathrm{irr}} - \Delta V},$$

where ΔV and V_{irr} are increasing volume and whole volume after irradiation. Fig. 3 shows the TEM observation results. Typical irradiation defects such as Frank dislocation loop or black dots were not observed.

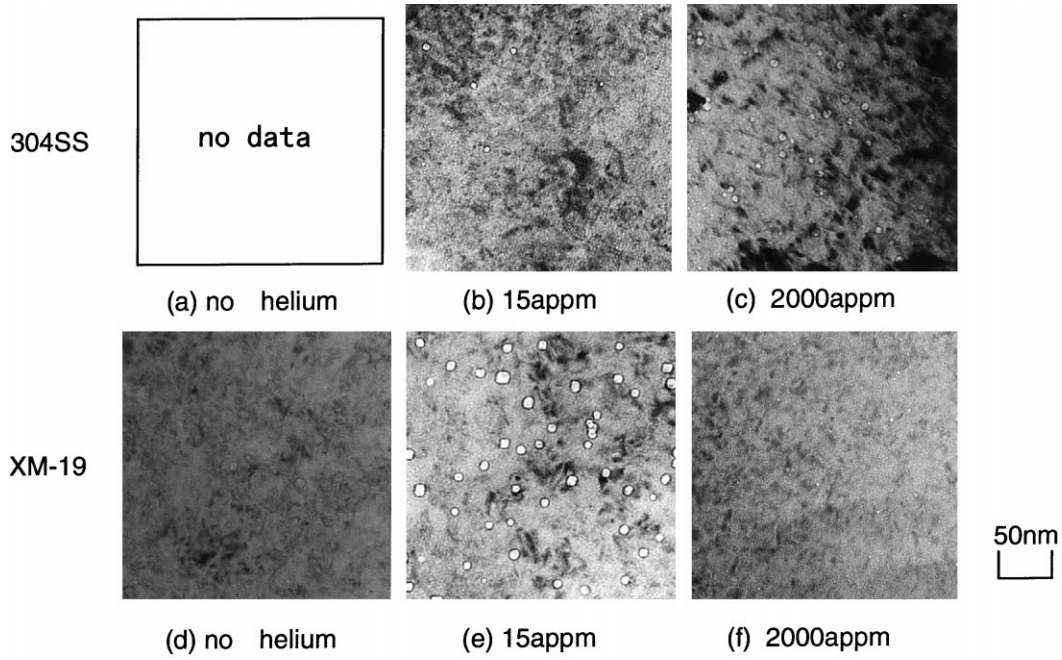

Fig. 3. The result of TEM observations of microstructure at various helium concentrations and alloy compositions. (a) 304SS only H_2^+ irradiated 1 dpa, (b) 304SS He^+ pre-injected 15 appm and H_2^+ irradiated 1 dpa, (c) 304SS He^+ pre-injected 2000 appm and H_2^+ irradiated 1 dpa, (d) 304SS only H_2^+ irradiated 1 dpa, (e) XM-19 He^+ pre-injected 15 appm and H_2^+ irradiated 1 dpa, (f) XM-19 He^+ pre-injected 2000 appm and H_2^+ irradiated 1 dpa.

However small cavities were observed in all irradiated samples. The density of the cavity in 304SS with 2000 appm He was higher than that in 304SS with 15 appm He. Similarly, XM-19 steel with 2000 appm He showed higher density of the cavity than XM-19 steel with 15 appm He. The average diameter of the cavity seen in XM-19 steel with 15 appm He was largest in this study. The average cavity size decreased with increasing the amount of pre-injected He contents. Swelling decreased with increasing of pre-injected He concentration in XM-19, however effect of He increasing was not detected in 304SS.

To clarify the effect of He pre-injection, a sample irradiated only by proton was prepared for XM-19 steel. Few cavities were recognized in it by TEM observation. The diameter of the cavity was slightly smaller than He pre-injected samples.

4. Discussion

4.1. Microchemical change

(a) *Effect of chemical composition on RIS.* Migration of alloy composition near grain boundaries results in RIS. The RIS is caused by super-saturated point defects, such as interstitial atom and vacancy sinking at grain boundary or surface. The phenomenon has been explained by the inverse Kirkendall effect or size effect of atoms. Some studies reported that these phenomenon were suppressed when over-sized atoms were contained in irradiated materials [6,7]. Thus in order to evaluate the behavior of over-sized element except Cr, XM-19 steel was chosen in this study as a test alloy containing over-sized Mn atom. In addition, to evaluate the effect of bulk Ni and Cr concentrations on segregation, test results for irradiated 304SS and XM-19 steel were compared.

The test results concerning XM-19 steel showed remarkable depression of Mn at grain boundary from 4.9 to 0.8 wt%, which seemed to affect segregation of other elements. The amount of Ni and Cr segregation in XM-19 steel was larger than that in 304SS. Increasing bulk Ni and Cr concentrations therefore enhanced the amount of segregation. Similar trends appeared in past studies [1,2].

(b) *Effect of irradiation temperature on RIS.* As mentioned in introduction part, degradation owing to irradiation seems to be not so active during irradiation under 400°C. However, RIS was observed for irradiated samples in this study. This result could suggest that accumulation of defects with low mobility took place at irradiation temperature of 300°C.

(c) *Effect of pre-injected He on RIS.* The data of grain boundary segregation are summarized in Table 3. The amount of Ni and Cr segregations tended to decrease with increasing pre-injected helium concentrations from 15 to 2000 appm in both steels, that is, samples including larger amount of pre-injected helium showed lower segregation. This should be because pre-injected helium behaved as defects sink for vacancy and interstitial.

(d) *Effect of irradiation particle on RIS.* The present results of RIS induced by He^+ and H_2^+ ion irradiation corresponded to RIS induced by neutron irradiation qualitatively but not quantitatively. Namely, the extent of RIS produced by He^+ and H_2^+ ion irradiation was larger than that produced by neutron irradiation, even at the same dpa [8].

The formation efficiency of fmd (freely migrating defect), which controls the diffusivity of the solute atom, was reported to be ten times higher with proton irradiation than with neutron irradiation [9–11]. Considering this difference in formation efficiency of fmd between proton and neutron irradiations, the amount of RIS in this study seems to correspond quantitatively to those by neutron irradiation [8].

4.2. Microstructural change

(a) *Dislocation density.* Typical irradiation defects, such as Frank loop or black dots were not observed, because intricately tangled network dislocations were already formed in the irradiated samples.

In the following, changes in dislocation density is compared between by proton irradiation in this study and by neutron irradiation in the literature [12].

In this study, the dislocation density for 304SS was 1×10^{11} cm^{-2} at displacement damage of 1 dpa by

Table 3
Summary of grain boundary segregation. The change in concentration (wt%)

Alloy type	Dose (dpa)	He concentration (appm)	Temperature (°C)	Concentration after irradiation (wt%)		
				Iron	Chromium	Nickel
304SS	1	15	300	71.4 → 70.8 ± 1.1	18.2 → 10.7 ± 1.2	8.7 → 16.8 ± 2.5
	1	2000	300	71.4 → 70.1 ± 0.8	18.2 → 11.3 ± 1.1	8.7 → 16.5 ± 2.4
XM-19	1	0	300	58.0 → 55.1 ± 0.3	21.9 → 10.6 ± 0.1	11.9 → 29.4 ± 0.2
	1	15	300	58.0 → 47.2 ± 0.4	21.9 → 6.7 ± 0.7	11.9 → 41.2 ± 0.6
	1	2000	300	58.0 → 56.0 ± 1.6	21.9 → 9.1 ± 0.6	11.9 → 33.8 ± 1.5

proton irradiation. On the other hand, in case of the neutron irradiation for similar solution-annealed austenitic stainless steel, it was reported that the dislocation density showed about 6×10^9 cm^{-2} at 1 dpa and about 6×10^{11} cm^{-2} at 10 dpa [12]. The latter corresponds to saturated dislocation density. Moreover, the dislocation density was almost similar (10^8 cm^{-2} order) for non-irradiated samples in these test. Accordingly, these results suggest that 1 dpa by proton irradiation almost corresponded to 10 dpa by neutron. Like the case of RIS, this effective displacement rates of proton irradiation seems to be related to the formation efficiency of fmd [9–11].

(b) *Cavities.* There was no cavity in XM-19 steels pre-injected only by He of 15 appm in the present authors' past experience. However, as shown in Fig. 3, cavities were observed in samples irradiated by H_2^+ or He^+ plus H_2^+ ions. Hence, observed cavities were related to displacement damage and accumulation of helium and hydrogen in the sample.

According to past studies [13,14] reporting the effect of pre-injected or simultaneously injected helium behavior in materials, density of voids tended to increase and diameter of voids tended to decrease compared with no helium pre-injection. This suggests that pre-injected helium decreases the energy of void nucleation and causes higher void density. In XM-19 steel sample with 2000 appm helium had larger cavity density compared with sample with 15 appm helium. Similar trend regarding cavity density was observed for 304SS samples with 2000 and 15 appm He. The present result showed good agreement with the past studies. A few cavities were observed in XM-19 sample irradiated only by proton. These results showed that formation of cavity was mainly caused by irradiation of H_2^+ but nucleation was affected by pre-injected helium.

(c) *Swelling.* Mobility of dislocation migration decreased with increasing bulk Ni contents [15]. Therefore reduction of void swelling occurred in materials with higher Ni contents. However, result of comparison between 304SS and XM-19 in this study indicated inverse trend to the past report. Cr increases the efficiency of dislocation migration relating to void swelling, this result seems to be caused by the effect of increment of Cr contents more conspicuous than increment of Ni contents.

5. Conclusions

1. Irradiation by 2 MeV H_2^+ at 300°C with pre-injection of 3 MeV He^+ at room temperature induced depletion of Cr and enrichment of Ni at grain boundaries in 304SS and XM-19 steels. This behavior was qualitatively the same as RIS by neutron irradiation. Considering the difference in formation efficiency of fmd, the amount of RIS observed in this study seems to correspond quantitatively to that by neutron irradiation.
2. The amount of Ni and Cr segregations increased with increasing bulk Ni and Cr compositions.
3. Cavities were observed in all irradiated conditions, namely, irradiations only by H_2^+ and by He^+ plus H_2^+. The cavity density increased when He contents increased in the sample, suggesting that helium plays an important role for nucleation of the cavity.

References

[1] D.L. Damcott et al., J. Nucl. Mater. 225 (1995) 97.
[2] H. Kinoshita et al., J. Nucl. Mater. 239 (1996) 205.
[3] E.A. Kenik, J. Nucl. Mater. 187 (1992) 239.
[4] J.P. Foster et al., J. Nucl. Mater. 224 (1993) 207.
[5] F.A. Garner et al., Proceedings of the Sixth International Symposium on Environmental Degradation of Materials in Nuclear Power Systems-Water Reactors, 1993, p. 783.
[6] N. Shigenaka, J. Nucl. Sci. Technol. 33 (7) (1996) 577.
[7] S. Kasahara, J. Nucl. Mater. 239 (1996) 194.
[8] K. Asano, K. Fukuya, Proceedings of the Fifth International Symposium on Environmental Degradation of Materials in Nuclear Power Systems-Water Reactors, 1992, p. 83.
[9] G.S. Was et al., Materials Characterization 32 (1994) 239.
[10] D.L. Damcott et al., Mater. Res. Soc. Symp. Proc. 373 (1995) 131.
[11] K. Fukuya, K. Nakata, Proceedings of the Fifth International Symposium on Environmental Degradation of Materials in Nuclear Power Systems–Water Reactors, p. 814.
[12] F.A. Garner, J. Nucl. Mater. 205 (1993) 98.
[13] Y. Murase et al., J. Nucl. Sci. Technol. 33 (3) (1996) 239.
[14] Y. Katoh et al., J. Nucl. Mater. 290–302 (1994) 210.
[15] W.G. Johnston et al., J. Nucl. Mater. 54 (1974) 24.